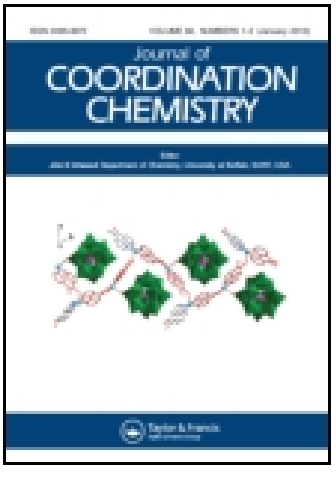

Journal of Coordination Chemistry
Publication details, including instructions for authors and subscription information:
http://www.tandfonline.com/loi/gcoo20

A new Wells-Dawson organic-inorganic hybrid polytungstate containing dimeric silver coordination complexes: $(Hpy)_2[Ag_2(phen)_4]_2(P_2W_{18}O_{62})$

Wu-Hua Chen[abc], Zhi-Biao Hu[c], Zhu-Sen Zhang[c], Le-Xing You[a], Shun-Ji Xie[a], Qiu-Lan Yuan[c], Jin-Hua Zhao[c], Tian-Fu Huang[c] & Jin-Xiao Mi[ab]

[a] College of Chemistry and Chemical Engineering, Xiamen University, Xiamen, PR China

[b] Fujian Provincial Key Laboratory of Advanced Materials, Department of Materials Science and Engineering, College of Materials, Xiamen University, Xiamen, PR China

[c] College of Chemistry and Material Science, Longyan University, Longyan, PR China

Accepted author version posted online: 25 Jul 2014.Published online: 20 Aug 2014.

To cite this article: Wu-Hua Chen, Zhi-Biao Hu, Zhu-Sen Zhang, Le-Xing You, Shun-Ji Xie, Qiu-Lan Yuan, Jin-Hua Zhao, Tian-Fu Huang & Jin-Xiao Mi (2014) A new Wells-Dawson organic-inorganic hybrid polytungstate containing dimeric silver coordination complexes: $(Hpy)_2[Ag_2(phen)_4]_2(P_2W_{18}O_{62})$, Journal of Coordination Chemistry, 67:15, 2583-2594, DOI: 10.1080/00958972.2014.948871

To link to this article: http://dx.doi.org/10.1080/00958972.2014.948871

Journal of Coordination Chemistry, 2014
Vol. 67, No. 15, 2583–2594, http://dx.doi.org/10.1080/00958972.2014.948871

A new Wells–Dawson organic–inorganic hybrid polytungstate containing dimeric silver coordination complexes: $(Hpy)_2[Ag_2(phen)_4]_2(P_2W_{18}O_{62})$

WU-HUA CHEN†‡§, ZHI-BIAO HU§, ZHU-SEN ZHANG§, LE-XING YOU†, SHUN-JI XIE†, QIU-LAN YUAN§, JIN-HUA ZHAO§, TIAN-FU HUANG§ and JIN-XIAO MI*†‡

†College of Chemistry and Chemical Engineering, Xiamen University, Xiamen, PR China
‡Fujian Provincial Key Laboratory of Advanced Materials, Department of Materials Science and Engineering, College of Materials, Xiamen University, Xiamen, PR China
§College of Chemistry and Material Science, Longyan University, Longyan, PR China

(*Received 10 April 2014; accepted 26 June 2014*)

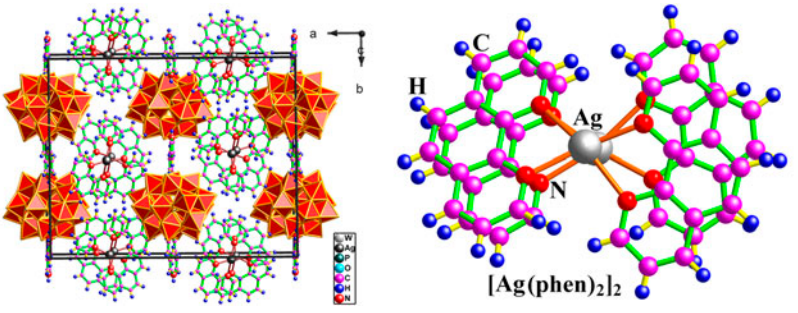

An effective route led to incorporating Ag^+ and reductive pyridine simultaneously into a polytungstate, which contains an uncommon dimeric Ag–coordination complex and mixed organic-ingredients.

An attempt to incorporate Ag^+ ions and some organic-reducing ingredients (e.g. pyridine) simultaneously into a polyoxometalate is a challenging task due to the high-standard reduction potential of Ag^+ ions. By using a second organic ligand to coordinate Ag^+ first, we prepared a new polytungstate, $(Hpy)_2[Ag_2(phen)_4]_2(P_2W_{18}O_{62})$ (**1**) (py = pyridine (C_5NH_5), phen = 1,10-phenanthroline ($C_{12}N_2H_8$)), which contains discrete inorganic polyanions ($[P_2W_{18}O_{62}]^{6-}$), protonated pyridine molecules, and $[Ag_2(phen)_4]^{2+}$ dimers. The isolated inorganic polyanions cluster close to the planes of (1 0 0) and are bound together by pyridine molecules via hydrogen bonds to form layers parallel to (1 0 0) at (0, *y*, *z*) and (0.5, *y*, *z*). The $[Ag_2(phen)_4]^{2+}$ dimers are located between successive layers of (1 0 0) and represent an uncommon feature that the hexagonal benzene rings of phen molecules are directly overlapped face to face. Our work opens a new way for synthesis of other Wells–Dawson organic–inorganic hybrid polytungstates by controlling reactant addition order.

Keywords: Hybrid polyoxometalate; Wells–Dawson structure; Hydrothermal synthesis; Polytungstate; Silver (Ag^+) ions

*Corresponding author. Email: jxmi@xmu.edu.cn

1. Introduction

Polyoxometalates (POMs), as one of the most important members in the family of solid-state chemistry, have architectural beauty and potential applications in catalysis, photochemistry, medicine, physical sciences, etc. [1–5]. Polytungstates are typical POMs which frequently consist of many classic polyanions, such as Keggin, Dawson, Anderson, and Waugh [6–10]. These polyanions are anticipated to play a crucial role as inorganic building blocks in the formation of functional 0-D–3-D organic–inorganic hybrid materials. Various organic–inorganic hybrid compounds based on Dawson-type heterpolyanions containing primary (central) heteroatoms (P^{V}, As^{V}, Si^{IV}, B^{III}, etc.) have been synthesized and reported [11–18].

Hydrothermal synthesis via the addition of organic ingredients (often acting as templates or structure-directing agents) gives various POMs. Introduction of organic groups into POMs could enrich the varieties of compounds, together with modulation of essential features, such as stability, bioavailability, and recognition [19, 20]. Bringing a second, even third organic group into POMs has gradually become a new research trend for new materials. Previous experiments show that 0-D POMs incorporating one organic ingredient rather than mixed ones readily are formed under hydrothermal reaction conditions even in the presence of several types of organic raw materials.

Hydrothermal synthesis is hardly predetermined, and affected by various factors including pH, stereo-hindrance, and organic ligand type rigid, e.g. bis(imidazole), bis(triazole) and flexible, e.g. 1,6-hexanediamine), as well as solubility of organic ligands in aqueous solution.

Introduction of transition metal elements (e.g. Ni^{II}, Zn^{II}, $Cu^{I/II}$, Co^{II}, and Cd^{II}) into POMs forming transition metal-substituted polyoxometalates (TMSPs) impacts their structures and properties, owing to the synergistic effect among inorganic building blocks and these metal complexes [21, 22]. Transition metals may act as (1) central atoms coordinating with organic ligands; as (2) succedaneums replacing high oxidation state atoms (e.g. $Mo^{V/VI}$, $W^{V/VI}$, $V^{IV/V}$, and Si^{IV}) in polyanions; as (3) bridges connecting with polyanions and organic ingredients; or as (4) nodes linking organic ligands to form 1-D–3-D frameworks. Ag has found applications in various materials owing to its excellent electroconductivity, plasma resonance performance, and sterilization activity [23–26]. However, POM-based extended structures containing Ag^{+} and/or Ag^{+} coordination complexes are comparatively unexplored [6, 27, 28]. Although numerous POM-based compounds modified by transition metal complexes (such as POM–Cu/Ni/Co/Zn system) have been synthesized and studied, few examples based on the POM–Ag system have been reported. Pyridine constitutes many metal–organic materials. To date only one POM, $[Ag(py)_2]_4[SiW_{12}O_{40}]$ [29] with Ag^{+} ions ligated by pyridine has been reported whereas silver complexes of $[Ag(py)_n]^{+}$ units are commonly found in other metal–organic compounds [30]. This may be due to the fact that free Ag^{+} ions have much higher standard reduction potential than Cu^{2+}, Cd^{2+}, Ni^{2+}, Co^{2+}, Zn^{2+}, etc. and readily transform into simple substances as Ag and Ag_2O, causing synthetic difficulties of Ag^{+} coordination complexes [15, 28, 31–35]. POMs with polymeric Ag coordination complexes containing Ag–Ag bonds are less found.

Based on ongoing work on related materials [36–39], we noticed that 1,10-phenanthroline ($C_{12}N_2H_8$ (phen)), unlike pyridine (C_5NH_5), coordinates (rather than reduce) with Ag^{+} to form stabilized $[Ag(phen)_n]^{+}$ units, from weak reducibility and strong coordination ability. By optimizing synthetic conditions (e.g. selection of organic reactants (pyridine and phen), sequence of adding reactants, and adjustment of pH values), we successfully

obtained a polytungstate, $(Hpy)_2[Ag_2(phen)_4]_2(P_2W_{18}O_{62})$ (**1**) under one-pot mild hydrothermal conditions. Various silver complexes of Wells–Dawson POMs with 4,4′-bipyridine have been reported previously [40] and a zinc complex of Wells–Dawson POMs with 1,10′-phenanthroline and 2-(5-phenylpyridin-2-yl)pyridine is also known [41]. Five compounds involving both Ag^+ coordinating with 1,10-phenanthroline and Ag···Ag clusters have been reported, including two coordination compounds ($[Ag_2\{\mu\text{-}Pr^iN(PPh_2)_2\}(1,10\text{-}phen)_2](NO_3)_2$ [42] and $[Ag_7(C_2)(CF_3CO_2)_5(phen)_5]\cdot 2CH_2Cl_2$ [43]) and three POMs (Ag-trimeric $[Ag(phen)_2]_3[Ag(phen)_3][AlW_{12}O_{40}]\cdot H_5O_2$ [6], $[Ag(phen)_3][Ag(phen)_2]_3[VW_{12}O_{40}]\cdot 4H_2O$ [44], and Ag-pentameric $[Ag(phen)_2]_7\{Ag[Ag(phen)(VW_{10}V_2O_{40})]_2\}$ [45]). However, no silver complexes of Wells–Dawson POMs containing both 1,10′-phenanthroline and pyridine have been reported.

Herein, we report the synthesis and structural characterization of $(Hpy)_2[Ag_2(phen)_4]_2(P_2W_{18}O_{62})$ (**1**), which contains the Wells–Dawson heteropolyanion, $[P_2W_{18}O_{62}]^{6-}$, and mixed organic units and dimeric $\{[Ag(phen)_2]_2\}^{2+}$ (figures 1 and 2). These results were confirmed by elemental analysis, energy-dispersive X-ray spectroscopy (EDS), powder X-ray diffraction (PXRD), Fourier transform infrared spectroscopy (FT-IR), Raman spectroscopy, and X-ray photoelectron spectroscopy (XPS) analyses. The thermal [thermogravimetry (TG)] and electrochemical [cyclic voltammetry (CV)] properties of **1** have also been studied.

2. Experimental

2.1. *General procedures*

All starting materials were purchased commercially and used as received. The elemental analysis was carried out on a Perkin-Elmer 2400 elemental analyzer (for C, H, and N).

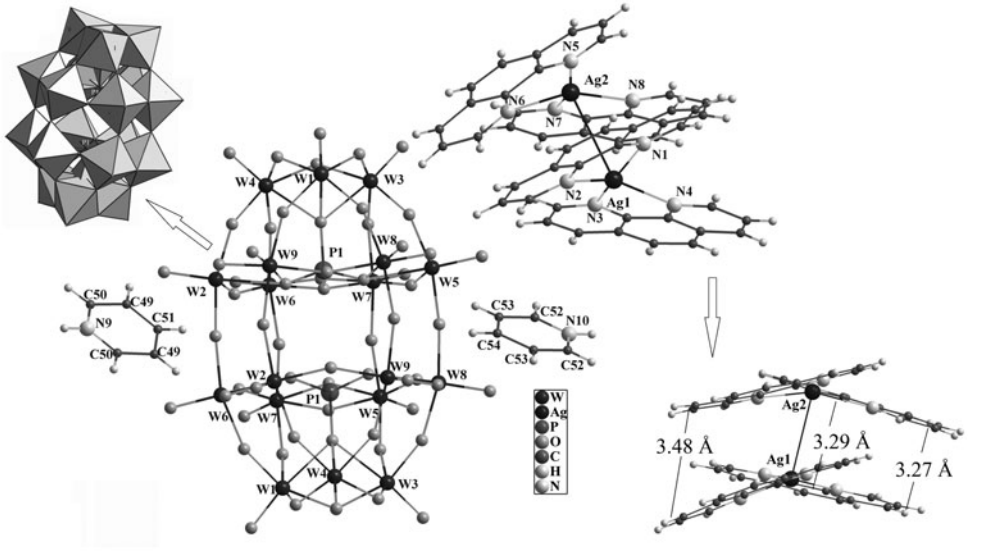

Figure 1. Fundamental building units in the asymmetric unit of $(Hpy)_2[Ag_2(phen)_4]_2(P_2W_{18}O_{62})$ (**1**). Left corner inset: the polyhedral representation of the $[P_2W_{18}O_{62}]^{6-}$ polyoxoanion. Right corner inset: the representation of $\{[Ag(phen)_2]_2\}^{2+}$ unit.

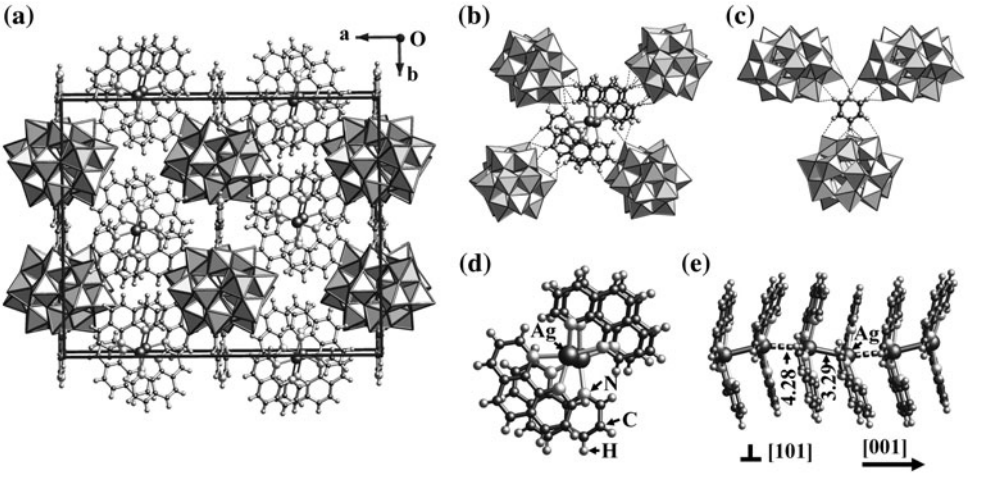

Figure 2. (a) The crystal structure of **1** viewed along the *c*-axis; (b) the linkage environments of $\{[Ag(phen)_2]_2\}^{2+}$ unit; (c) the linkage environments of pyridine unit; (d) one pair of phen groups in $[Ag(phen)_2]_2\}^{2+}$ dimer, hexagons of the top phen group are directly located above the hexagons of the bottom phen group; and (e) the display of the zig–zag arrangement of Ag···Ag "chain" running along the *c*-axis, viewed down along the direction of [1 0 1].

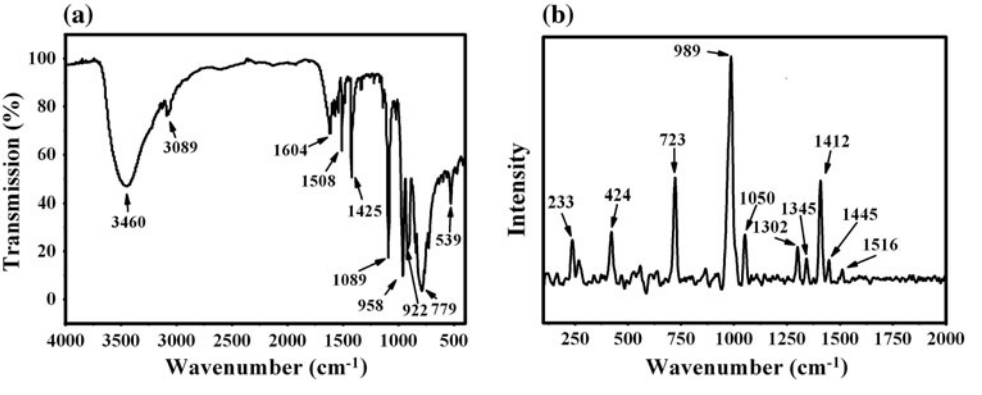

Figure 3. (a) FT-IR spectrum of **1** and (b) Raman spectrum of **1**.

PXRD data were collected on a Philips X'Pert-PRO X-ray diffractometer with Cu *Kα* radiation ($\lambda = 1.54178$ Å) (figure S1, see online supplementary material at http://dx.doi.org/10.1080/00958972.2014.948871). The morphology and the EDS of the synthesized compound were recorded with a Leo 1530 Field Emission Scanning Electron Microscope (figures S2 and S3). The FT-IR spectrum (KBr pellets) was recorded on a Nicolet Impact 410 FTIR from 400 to 4000 cm^{-1} [figure 3(a)]. FT-Raman spectra were measured using a BRUKER 110/S spectrometer [figure 3(b)]. Both IR and Raman spectra were recorded with a spectral resolution of 2 cm^{-1}. XPS analysis was performed using a physical electronics quantum 2000 scanning ESCA microprobe with a standard-focused monochromatic Al Kα (1486.7 eV) X-ray source (figures S5–S7). Thermogravimetric analysis was performed in flowing N_2 from 30 to 950 °C on a TG 209 F1 thermogravimetric analyzer at a heating rate of 10 °C min^{-1} [figure 4(a)]. CV data were recorded on a CHI 660 electrochemical

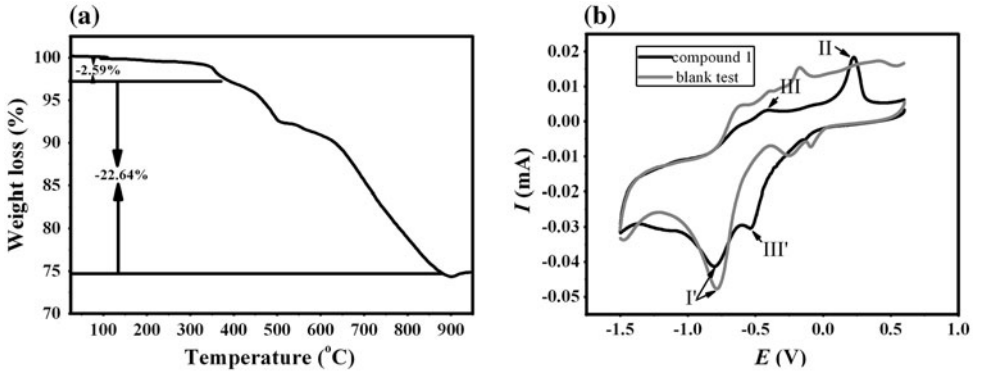

Figure 4. (a) TG curve of **1** in N_2 atmosphere and (b) cyclic voltammograms of **1** and blank test performed in the DMSO containing 0.1 M $NaClO_4$. Conditions: concentration ~5 × 10^{-4} M; scan rate 50 mV s^{-1}; and reference electrode Ag/AgCl.

workstation, which is connected to a Digital-XP personal computer used for control of the electrochemical measurements and data collection [figure 4(b)]. A three-electrode system was used. The working electrode was a modified carbon-paste electrode. A Ag/AgCl (saturated KCl) electrode was used as a reference electrode and a Pt gauze as a counter electrode.

2.2. *Synthesis and initial characterization*

In a typical synthesis, a mixture of $AgNO_3$ (0.12 g, 0.71 mM), 1,10-phenanthroline ($C_{12}N_2H_8$) (0.28 g, 1.4 mM), distilled water (H_2O) (20 mL, 1.1 M), Na_2WO_4 (2.06 g, 0.7 mM), H_3PO_4 (0.6 mL 85%, 9.6 mM), and pyridine (C_5NH_5) (1.0 mL, 12.4 mM) in a molar ratio of ~1 : 2 : 1500 : 1 : 14 : 18 was prepared by adding reactants in the given order, and sealed in a 30 mL Teflon-lined stainless steel autoclave with *ca.* 70% filling. Then the resulting gel, with a pH of ~5.5, was heated to and held at 170 °C in an oven for 3.5 days. Finally, it was cooled at a rate of *ca.* 10 °C h^{-1} to room temperature. The resultant products, which contained a mixture of powder and yellow monoclinic crystals, were recovered by filtration, washed with distilled water, and dried in air at ambient temperature (63% yield based on W). The manually selected crystals gave chemical compositions: (1) Anal. Calcd (wt %) for **1**: W, 51.74; Ag, 6.76; P, 0.97; H, 1.19; N, 3.94; C, 19.89; O, 15.51 and (2) found (wt %): H, 1.33; N, 3.76; C, 20.01.

The synthesis conditions of **1** are very tricky. The order of adding reactants is a key factor for synthesizing **1**. The $AgNO_3$, 1,10-phenanthroline, and distilled water should be mixed first. After aging *ca.* 30 min, Na_2WO_4 and H_3PO_4 were then added. The reductive pyridine should be put in at the last step under continual stirring. Otherwise, due to free Ag^+ ions being reduced, the major products were, instead of **1**, white Ag-elementary substance, organic remnants, and some colorless crystal materials (namely $(C_5NH_6)_{4.5}(H_3O)_{1.5}[P_2W_{18}O_{62}]$ (**2**) [46], which contains no Ag-coordination complex and only one organic ingredient). Also, the reaction is pH-value-dependent. H_3PO_4 and organic reagents were used to adjust the pH of the reaction system. Crystals of **1** were only obtained at pH 4–7. For pH ≥ 7, colorless crystals of **2** were obtained instead. With temperatures from 130 to 190 °C with intervals of 10°, the best reaction temperature was 160–170 °C for

1. Under the above conditions POMs adopt the Wells–Dawson structure. However, the mechanism of formation is not clear. Attempts to synthesize pure **1** under various conditions were not successful. The samples used for detailed characterizations were handpicked under a microscope. The identity and purity of the selected samples have been confirmed by PXRD patterns (figure S1).

2.3. *Single-crystal structure determination*

A suitable single crystal (0.22 mm × 0.18 mm × 0.15 mm) of **1** was carefully selected under an optical microscope and glued on a thin glass fiber with epoxy resin. Single-crystal X-ray diffraction (XRD) data were collected by using oscillation frames from $\theta = 0.99°$ to 28.37° on a Rigaku RAXIS-IV image plate area detector equipped with graphite-monochromated Mo Kα ($\lambda = 0.71073$ Å) radiation using a $\omega - \varphi$ scan mode at room temperature. The structure was solved in the space group *C2/c* (No. 15) by direct methods and refined on F^2 by full-matrix least-squares using SHELX-97 [47]. The non-hydrogen atoms were refined anisotropically and hydrogens isotropically. All hydrogens were generated geometrically. A summary of crystallographic data and structure refinement for **1** is listed in table 1 and deposited in the Cambridge Crystallographic Data Center with CCDC No. 978794. Selected bond lengths and angles are given in table 2. Fractional atomic coordinates, isotropic or equivalent isotropic displacement parameters, and anisotropic atomic displacement parameters (Å^2) are given in tables S1 and S2, respectively.

3. Results and discussion

3.1. *Structure descriptions*

Single-crystal XRD reveals that the asymmetric unit of **1** consists of one discrete $[P_2W_{18}O_{62}]^{6-}$ polyanion, two $[Ag_2(1,10\text{-phenanthroline})_4]^{2+}$, and two protonated pyridine

Table 1. Crystal data and structure refinement for $(Hpy)_2[Ag_2(phen)_4]_2(P_2W_{18}O_{62})$ (**1**).

Empirical formula	$C_{106}H_{76}Ag_4N_{18}O_{62}P_2W_{18}$
Formula weight	6396.39
Temperature (K), Wavelength (Å)	293(2), 0.71073
Crystal system, space group	Monoclinic, *C2/c* (No. 15)
a (Å)	33.030(4)
b (Å)	26.564(2)
c (Å)	14.7007(19)
β (°)	98.200(2)
Volume (Å^3)	12,766(3)
Z, D_{Calcd} (g cm^{-3})	4, 3.328
μ (mm^{-1}), *F* (0 0 0)	16.866, 11,536.0
Crystal size (mm), color	0.22 × 0.18 × 0.15, yellow
θ range (°)	2.30–28.33
Limiting indices	$-42 \le h \le 42$, $-35 \le k \le 33$, $-19 \le l \le 19$
Reflections collected	53,870
Independent reflections	15,112 [R(int) = 0.0574]
Refinement method	Full-matrix least-squares on F^2
Data/restraints/parameters	13,403/0/900
Goodness of fit on F^2	1.069
Final *R* indices [$I > 2\sigma(I)$]	$R_1 = 0.0508$, $wR_2 = 0.1277$
R indices (all data)	$R_1 = 0.0574$, $wR_2 = 0.1319$
Largest diff. peak and hole (e Å^{-3})	3.644 and –4.750

Table 2. Selected bond lengths (Å) and angles (°) for **1**.

Bond	Dist.	Bond	Dist.	Bond	Dist.
W(1)–O(8)	1.705(7)	W(4)–O(2)	2.364(6)	W(8)–O(17)^{i}	1.930(6)
W(1)–O(28)	1.882(7)	W(5)–O(5)	1.698(7)	W(8)–O(7)	2.362(6)
W(1)–O(23)	1.908(6)	W(5)–O(3)	1.889(6)	W(9)–O(12)	1.709(7)
W(1)–O(29)	1.912(7)	W(5)–O(22)	1.905(7)	W(9)–O(11)^{i}	1.890(6)
W(1)–O(31)	1.951(7)	W(5)–O(30)	1.909(6)	W(9)–O(18)^{i}	1.907(7)
W(1)–O(2)	2.374(6)	W(5)–O(6)	1.911(7)	W(9)–O(27)	1.919(7)
W(2)–O(15)	1.702(7)	W(5)–O(9)	2.354(6)	W(9)–O(14)	1.935(7)
W(2)–O(24)	1.879(6)	W(6)–O(10)	1.696(7)	W(9)–O(7)	2.381(6)
W(2)–O(11)	1.897(6)	W(6)–O(19)	1.883(7)	Ag(1)–N(2)	2.291(10)
W(2)–O(13)	1.901(7)	W(6)–O(23)^{i}	1.897(6)	Ag(1)–N(3)	2.318(9)
W(2)–O(25)	1.925(6)	W(6)–O(24)	1.916(6)	Ag(1)–N(4)	2.377(9)
W(2)–O(16)	2.331(6)	W(6)–O(13)^{i}	1.921(7)	Ag(1)–N(1)	2.412(9)
W(3)–O(20)	1.703(7)	W(6)–O(16)^{i}	2.382(6)	Ag(1)–Ag(2)	3.2907(1)
W(3)–O(17)	1.881(6)	W(7)–O(1)	1.695(7)	Ag(2)–N(5)	2.244(9)
W(3)–O(6)	1.902(7)	W(7)–O(14)	1.862(7)	Ag(2)–N(7)	2.311(9)
W(3)–O(26)	1.913(6)	W(7)–O(30)	1.890(6)	Ag(2)–N(8)	2.313(9)
W(3)–O(29)	1.921(7)	W(7)–O(19)^{i}	1.902(6)	Ag(2)–N(6)	2.402(9)
W(3)–O(2)	2.394(6)	W(7)–O(28)	1.954(7)	P(1)–O(7)^{i}	1.519(6)
W(4)–O(21)	1.720(7)	W(7)–O(9)	2.371(6)	P(1)–O(9)	1.521(6)
W(4)–O(31)	1.883(6)	W(8)–O(4)	1.708(7)	P(1)–O(16)	1.532(6)
W(4)–O(25)	1.902(6)	W(8)–O(22)	1.893(7)	P(1)–O(2)	1.567(7)
W(4)–O(18)	1.911(7)	W(8)–O(3)^{i}	1.898(6)		
W(4)–O(26)	1.926(7)	W(8)–O(27)	1.901(6)		
Angle	(°)	Angle	(°)	Angle	(°)
N(2)–Ag(1)–N(3)	120.1(3)	N(5)–Ag(2)–N(7)	161.8(3)	O(7)^{i}–P(1)–O(9)	111.2(4)
N(2)–Ag(1)–N(4)	150.8(3)	N(5)–Ag(2)–N(8)	118.9(3)	O(7)^{i}–P(1)–O(16)	111.6(4)
N(3)–Ag(1)–N(4)	71.3(3)	N(7)–Ag(2)–N(8)	72.7(3)	O(9)–P(1)–O(16)	111.7(4)
N(2)–Ag(1)–N(1)	71.8(3)	N(5)–Ag(2)–N(6)	72.9(3)	O(7)^{i}–P(1)–O(2)	107.1(4)
N(3)–Ag(1)–N(1)	166.8(3)	N(7)–Ag(2)–N(6)	101.4(3)	O(9)–P(1)–O(2)	107.7(4)
N(4)–Ag(1)–N(1)	101.3(3)	N(8)–Ag(2)–N(6)	158.1(3)	O(16)–P(1)–O(2)	107.2(3)
N(2)–Ag(1)–Ag(2)	88.1(2)	N(5)–Ag(2)–Ag(1)	97.1(3)	P(1)–O(2)–W(4)	125.8(4)
N(3)–Ag(1)–Ag(2)	85.6(2)	N(7)–Ag(2)–Ag(1)	100.2(2)	P(1)–O(2)–W(1)	124.5(3)
N(4)–Ag(1)–Ag(2)	120.7(2)	N(8)–Ag(2)–Ag(1)	71.0(2)	P(1)–O(2)–W(3)	124.3(3)
N(1)–Ag(1)–Ag(2)	89.2(3)	N(6)–Ag(2)–Ag(1)	89.8(2)	W(4)–O(2)–W(1)	90.4(2)

Note: Symmetry code: (i) $-x + 1, y, -z + 1/2$.

cations ($[C_5NH_6]^+$) (figure 1). The isolated inorganic polyanions ($[P_2W_{18}O_{62}]^{6-}$) cluster close to the planes of (1 0 0), forming a layer at the sites of (0, *y*, *z*) and (0.5, *y*, *z*), respectively [figure 2(a)]. Pyridine molecules are dispersed within the layers of inorganic polyanions while $[Ag_2(phen)_4]^{2+}$ dimers are located between successive layers. The 0-D structural setup is stabilized by hydrogen bonds among these discrete constituents.

The classical Wells–Dawson polyoxoanion, $[P_2W_{18}O_{62}]^{6-}$, contains two identical $[\alpha\text{-}PW_9O_{31}]^{3-}$ units which can be derived from the well-known Keggin $[\alpha\text{-}PW_{12}O_{40}]^{6-}$ anions by removal of a set of three corner-sharing WO_6 octahedra. The $[P_2W_{18}O_{62}]^{6-}$ anion in **1** deviates significantly from the regular form with symmetry $\bar{6}m2$–D_{3h}, and shows only twofold symmetry in the horizontal. Each moiety contains a $[PO_4]$ tetrahedron in center, three base corners which are corner-sharing with an octahedral edge-shared $[W_2O_{10}]$ dimer (i.e. to a six-tungsten-membered ring), and the rest upward apex sharing with an octahedral edge-shared $[W_3O_{13}]$ trimer (figure 1). All nine coordination polyhedra of crystallographic distinct W exhibit a $\{WO_6\}$ distortedly octahedral environment in which W–O distances are 1.695(7)–1.720(7) Å for terminal oxygens (W–O_t), 1.879(6)–1.951(7) Å for μ_2-bridging oxygens (corner-sharing W–O_c and edge-sharing W–O_e), and 2.331(6)–2.394(6) Å for μ_3-bridging oxygens (O bonded to two or three W and one P W–O_i). All of them are in the

normal ranges. The bond valence sum (BVS) calculations on the tungstate sites give the values 6.18, 6.37, 6.27, 6.20, 6.33, 6.31, 6.37, 6.26, and 6.16 for W(1), W(2), W(3), W(4), W(5), W(6), W(7), W(8), and W(9), respectively, with an average value of 6.27 [48]. Moreover, the BVS calculations give the value 4.83 for *P*(1). This clearly indicates that the nine independent tungstens are +6 and the central *P* are +5. The P–O bond lengths vary between 1.519(6) and 1.567(7) Å, while the O–P–O angles are in the normal range of 107.1(4)°–111.7(4)°, as observed in our previous report [49].

The 1,10-phenanthroline molecules coordinated with Ag ions forming the $\{[Ag(phen)_2]_2\}^{2+}$ fragment, while the pyridine molecules are protonated. $\{[Ag(phen)_2]_2\}^{2+}$ exhibits an array like a double propeller of a helicopter (figure 1). This dimer, $\{[Ag(phen)_2]_2\}^{2+}$, consists of two silver ions and four phen molecules, parallel arranged by face-to-face mode. These two sets of phen molecules are pinned together angularly (~148.2°) by a pair of silver ions. The distances between parallel planes of two pairs of phen groups are *ca.* 3.27 and 3.48 Å, respectively, while that between Ag(1) and Ag(2) is 3.29 Å, shorter than the sum of the van der Waals radii of two silver ions (3.44 Å). The Ag–Ag distance (at 3.29 Å) of dimeric $\{[Ag(phen)_2]_2\}^{2+}$ in **1** is comparable with those (at 3.31 Å) in two trimeric $\{[Ag(phen)_2]_3\}^{3+}$ compounds [6, 44], but significantly shorter than those (at 3.35–3.39 Å) observed in a pentameric $\{[Ag(phen)_2]_5\}^{5+}$ compound [45] (figure S4). The dimers $\{[Ag(phen)_2]_2\}^{2+}$ have hexagons of the top phen directly located above the hexagons of the bottom phen [figure 2(d)]. This feature is also observed in two trimeric $\{[Ag(phen)_2]_3\}^{3+}$ compounds [6, 44], but none of the phen groups in the pentameric $\{[Ag(phen)_2]_5\}^{5+}$ is directly located above the hexagons of other phen [45]. All neighboring phen groups in this report as well as in silver trimeric and pentameric compounds [6, 44, 45] are aligned in a parallel or nearly parallel mode, differing from the common arrangement of organic molecules in other Ag POMs [50] (figure S4). A closer inspection of the dinuclear silver cluster reveals that intermolecular π–π interactions between phen ligands play an important role in stabilization of the dimeric $\{[Ag(phen)_2]_2\}^{2+}$.

The crystal structure of **1** can be envisaged as discrete inorganic polyoxoanions ($[P_2W_{18}O_{62}]^{6-}$), organic compensating cations (protonated pyridine ($[C_5NH_6]^+$)), and organic–inorganic hybrid cations ($\{[Ag(phen)_2]_2\}^{2+}$) arranged in a close packing. The Wells–Dawson polyoxoanion $[P_2W_{18}O_{62}]^{6-}$ groups, like prolate ellipsoids of revolution, tilting in space and extending their longest axis along the direction of [1 0 $\bar{3}$], cluster close to the (1 0 0) planes at the sites (0, *y*, *z*) and (0.5, *y*, *z*), respectively [figure 2(a)]. Moreover, the $\{[Ag(phen)_2]_2\}^{2+}$ dimers are located around $x = 1/4$ or $x = 3/4$ between successive layers, which consist of isolated polyoxoanion $[P_2W_{18}O_{62}]^{6-}$ ellipsoids. Each $[P_2W_{18}O_{62}]^{6-}$ ellipsoid in the plane of (1 0 0) links to its four nearest-neighbor counterparts by two opposite, protonated pyridine (Hpy) molecules via hydrogen bonds. Therefore, each protonated pyridine is bound by three polyoxoanion ellipsoids and the planes of pyridine groups nearly parallel to the plane of (1 0 0) [figure 2(a) and (c)]. In contrast, each $\{[Ag(phen)_2]_2\}^{2+}$ dimer is surrounded by four polyoxoanion ellipsoids [figure 2(b)]. All phen groups of $\{[Ag(phen)_2]_2\}^{2+}$ dimers are arranged approximately parallel to the direction of [1 0 1] and nearly perpendicular to [0 0 1] direction [figure 2(e)]. In the $[Ag(phen)_2]^+$ fragment, the center Ag and its four coordination N, afforded by two phen ligands, display somewhat distorted rectangle configuration. In the oblong $\{AgN_4\}$, the distances of Ag–N and the angles of N–Ag–N are 2.291(10)–2.449(9) Å and 71.3(3)°–166.8(3)°, respectively. The arrangement of neighboring $\{[Ag(phen)_2]_2\}^{2+}$ dimers displays an interesting zig–zag configuration of Ag–Ag···Ag–Ag···"chain" with a spacing at 3.29 or 4.28 Å alternately running along

the *c*-axis [figures 2(e) and S4(a)], which differs from the Ag-pentameric chain with approximately equal spacing (at 3.35–3.39 Å) [figure S4(c)].

3.2. *FT-IR and Raman spectrum*

In the FT-IR spectrum of **1**, bands at 1000–700 cm^{-1} show the characteristic polyoxoanion Dawson structure [51]. As shown in figure 3(a), the band at *ca.* 958 cm^{-1} corresponds to the characteristic W=O_t stretch and those at *ca.* 922, 779 cm^{-1} to the asymmetric stretch of W–$O_{\mu 2,3}$–W (herein, $O_{\mu 2}$ for μ_2-bridging oxygens and $O_{\mu 3}$ for μ_3-bridging oxygens). The bands at 1089 and 539 cm^{-1} can be attributed to the ν_3 antisymmetric stretching mode and the ν_4 asymmetric bending mode of PO_4^{3-}, respectively [52], while those at 1604, 1508, and 1425 cm^{-1} are assigned to bending vibrations of 1,10-phenanthroline and pyridine. The intense broad peak at *ca.* 3460 cm^{-1} with a shoulder at 3089 cm^{-1} is assigned to stretching vibrations of N–H and C–H of py and phen.

In the Raman spectrum [figure 3(b)], the weak band at 233 cm^{-1} and strong band at 989 cm^{-1} can be assigned to bending vibrations and stretching vibrations of terminal W=O_t, respectively, while the peaks at *ca.* 424 and 723 cm^{-1} can be attributed to bending vibrations and stretching vibrations of the W–$O_{\mu 2,3}$–W groups, respectively [53]. The peak at 1050 cm^{-1} can be attributed to v_3 (PO_4^{3-}) antisymmetric stretching vibrations and the relative weak peaks at *ca.* 1302–1516 cm^{-1} are assigned to bending vibrations of organic groups.

3.3. *XPS spectroscopy*

XPS spectral investigations of **1** were performed to further demonstrate the chemical composition and the oxidation state of elements. As shown in figure S5, peaks at 35.54 and 37.64 eV in the W4*f* region can be attributed to $W^{6+}(4f_{7/2})$ and $W^{6+}(4f_{5/2})$, respectively [54]. Figure S6 shows the peak at 1136.33 eV can be ascribed to $Ag^{+}(3d_{5/2})$, while the peak at 133.20 eV in figure S7 can be ascribed to $P^{5+}(2p_{3/2})$ [54]. The assignment of XPS spectra proves the composition of **1** as described above.

3.4. *Thermal properties*

The thermogravimetric investigations of $(Hpy)_2[Ag_2(phen)_4]_2(P_2W_{18}O_{62})$ (**1**) were performed in flowing N_2 from 30 to 950 °C. As shown in figure 4(a), the TG curve of **1** exhibits three weight loss steps. The first weight loss (2.59 wt%) from 150 to 337 °C is attributed to release of $[C_5NH_6]^+$ (Calcd 2.50 wt%). The continuous second and third weight losses at 392–525 and 525–898 °C can be attributed to decomposition of $\{[Ag(phen)_2]_2\}^{2+}$ and framework of the polyanions (22.64 wt% *versus* Calcd 22.52 wt%). It indicates that the processes of decomposition of organonitrogen ligand (phen) are stepwise. The total weight loss (25.23 wt%) agrees with the calculated value (Calcd 25.02 wt%) for removal of all organic molecules. These results support the chemical composition of **1** from the above crystal structure analysis. The multiple step release of organic groups proves the 1,10-phenanthroline coordinates with Ag^+ (*versus* pyridine). An attempt to identify the residue after thermal decomposition by XRD was not successful, owing to amorphization of the material.

3.5. *Electrochemical studies*

CV was used to study **1** in DMSO in the presence of 0.1 M $NaClO_4$ as a supporting electrolyte and in the potential range from +0.6 to –1.5 V. As shown in figure 4(b), there is a common cathodic peak at –0.80 V (I′) (vs. Ag/AgCl), attributed to the redox processes of DMSO. By comparison with the blank test, the experimental results show that a pair of reversible redox peaks at –0.42 V(III) and –0.54 V (III′), with mean peak potential $E_{1/2} = (E_{pa} + E_{pc})/2$ is –0.48 V, can be attributed to the one-electron process of tungstate [6, 11, 35, 55]. There is an additional irreversible anodic peak (II) located at +0.23 V, which should be assigned to oxidation of Ag (+I) [56]. No obvious cathodic peak corresponding to II, but a cathodic peak (III′) corresponding to III, has been observed, indicating that the polyanion $[P_2W_{18}O_{62}]^{6-}$ reveals certainly oxidizability in DMSO. The dimeric silver complexes can be reduced, but Ag(0) is not re-oxygenated in the same conditions. CV measurements in this report are somewhat different from the typical CV curves for Wells–Dawson polyoxotungstates [57]. This may arise from its complicated chemical constituents and different measurement conditions.

3.6. *Discussion*

There are only three POMs/TMSPs previously reported, which contain Ag^+ with 1,10-phenanthroline and further forming Ag···Ag clusters [6, 44, 45]. Moreover, only one polytungstate with hybrid Ag^+ ions ligated by pyridine molecules has been reported [29]. Herein, we introduced a second organic molecule (i.e. pyridine) into polytungstate besides $[Ag_2(phen)_4]^{2+}$ dimers. The scarcity may be due to the fact that free Ag^+ ions readily transform to Ag or Ag_2O in solution with reducing organic molecules. The formation of **1** arises from control of the reactant addition sequence. Under continual stirring, Ag ions coordinate with 1,10-phenanthroline first, then are mixed with the reducing substances (i.e. pyridine), weakening the effect of free Ag^+ ions being reduced. Another key factor for the experiments is selecting the types of nitrogenous organic reactants. Two organic reactants, i.e. C_5NH_5 (pyridine) and $C_{12}N_2H_8$ (1,10-phenanthroline) were chosen to synthesize related materials, which improved the solubility of organic ingredients in aqueous solution and took stereo-hindrance effect into account. The advantage of using liquid organic micromolecule (pyridine) is the fact that the organic ligands can be better dispersed in aqueous solution.

An attempt to incorporate Ag^+ and organic-reducing ingredients (e.g. pyridine) simultaneously into a complex is challenging due to the fact that silver (Ag^+) ions have high-standard reduction potential at +0.80 V for $Ag^+(aq) + e^- \rightarrow Ag(s)$, which is much higher than those of Cu^{2+}(+0.34 V), Ni^{2+}(–0.25 V), Co^{2+}(–0.28 V), Cd^{2+}(–0.40 V), Fe^{2+}(–0.44 V), and Zn^{2+}(–0.76 V). So the Ag^+ ions have a greater likelihood of being reduced when mixed with organic-reducing ingredients, such as pyridine. The CV investigation shows that the reduction potential of $Ag^+(aq) + e^- \rightarrow Ag(s)$ negatively shift at +0.23 V (much lower than its standard reduction potential, +0.80 V) after Ag^+ coordinates with 1,10-phenanthroline. This result demonstrates that Ag-coordination complexes are harder to reduce than free Ag^+ ions. The synthesis of **1** provides an example that selecting organic ligands and adjusting subtle factors, such as the order of adding reactants, pH, and reagents ratio of the reaction system, may be an essential approach to acquire a novel configuration POM. Previous report indicates that Ag^+ ions can coordinate directly with pyridine derivatives such as 4,4′-bipyridine in Wells–Dawson POMs [40], suggesting that the reducing ability of 4,4′-bipyridine should be less than pyridine. The only known polytungstate $[Ag(py)_2]_4[SiW_{12}O_{40}]$,

that has Ag^+ ions ligated by pyridine, was synthesized from pyridine-2,6-dicarboxylate as a starting material, which decomposed completely to pyridine in the presence of Ag^+ [29].

4. Conclusion

We report synthesis and characterization of a new Wells–Dawson POM, $(Hpy)_2[Ag_2(phen)_4]_2(P_2W_{18}O_{62})$ (**1**), which contains $\{[Ag(phen)_2]_2\}^{2+}$ and two types of organonitrogen units. The key factors of the synthetic procedures have been well established, which include reagents, ratio, and pH. Particularly, reactant addition sequence is crucial, which promotes Ag^+ ions ligating with ligands before being reduced by organic-reducing reagents. Thermal properties further confirm that two different organic reactants (i.e. phen and py) played different roles in formation and stability of **1**. Reactant addition sequence which the present work emphasized may become an effective strategy for construction of multinuclear subunit-based MOFs of transition metals with high-standard reduction potential (e.g. Ag^+ and Cu^{2+}).

Funding

This work was supported by the Foundation of Education Department of Fujian Province, PR China [grant number JB12199], [grant number JA11245]; the National Natural Science Foundation of China [grant number 21233004], [grant number 40972035].

References

[1] C.L. Hill. *Chem. Rev.*, **98**, 1 (1998).
[2] C.L. Hill, C.M. Prosser-McCartha. *Coord. Chem. Rev.*, **143**, 407 (1995).
[3] D.J. Chesnut, D. Hagrman, P.J. Zapf, R.P. Hammond, R. LaDuca, R.C. Haushalter, J. Zubieta. *Coord. Chem. Rev.*, **190–192**, 737 (1999).
[4] G. Liu, T.B. Liu, S.S. Mal, U. Kortz. *J. Am. Chem. Soc.*, **128**, 10103 (2006).
[5] Y. Nakagawa, K. Uehara, N. Mizuno. *Inorg. Chem.*, **44**, 14 (2005).
[6] L. Yuan, C. Qin, X.L. Wang, Y.G. Li, E.B. Wang. *J. Chem. Soc., Dalton Trans.*, 4169 (2009).
[7] D.W. Yan, Q. Chen, Y. Xu, Q. Sun, D.R. Zhu, Y. Song, S.P. Elangovan. *Inorg. Chem. Commun.*, **14**, 1314 (2011).
[8] R. Cao, K.P. O'Halloran, D.A. Hillesheim, K.I. Hardcastle, C.L. Hill. *CrystEngComm*, **12**, 1518 (2010).
[9] J. Liu, J.N. Xu, Y.B. Liu, Y.K. Lu, J.F. Song, X. Zhang, X.B. Cui, J.Q. Xu, T.G. Wang. *J. Solid State Chem.*, **180**, 3456 (2007).
[10] J.H.B. Wu, Y.L. Xu, K. Yu, Z.H. Su, B.B. Zhou. *J. Coord. Chem.*, **66**, 2821 (2013).
[11] M. Ammam, J. Fransaer. *J. Solid State Chem.*, **184**, 818 (2011).
[12] P.J.S. Richardt, R.W. Gable, A.M. Bond, A.G. Wedd. *Inorg. Chem.*, **40**, 703 (2001).
[13] C. Liang, Y. Lu, H. Fu, W.L. Chen, E.B. Wang. *J. Coord. Chem.*, **65**, 3254 (2012).
[14] H. Fu, Y.G. Li, Y. Lu, W.L. Chen, Q.O. Wu, J.X. Meng, X.L. Wang, Z.M. Zhang, E.B. Wang. *Cryst. Growth Des.*, **11**, 458 (2011).
[15] P.P. Zhang, J. Peng, H.J. Pang, J.Q. Sha, M. Zhu, D.D. Wang, M.G. Liu, Z.M. Su. *Cryst. Growth Des.*, **11**, 2736 (2011).
[16] A.X. Tian, X.L. Lin, N. Sun, Y.J. Liu, Y. Yang, J. Ying. *J. Coord. Chem.*, **67**, 495 (2014).
[17] C.L. Wang, Y.H. Ren, S.J. Feng, Z.P. Kong, Y.C. Hu, B. Yue, M.L. Deng, H.Y. He. *J. Coord. Chem.*, **67**, 506 (2014).
[18] Y.L. Xu, K. Yu, B.B. Zhou, Z.H. Su, J. Wu. *J. Coord. Chem.*, **66**, 1303 (2013).
[19] J.T. Rhule, C.L. Hill, D.A. Judd, R.F. Schinazi. *Chem. Rev.*, **98**, 327 (1998).
[20] S. Bareyt, S. Piligkos, B. Hasenknopf, P. Gouzerh, E. Lacôte, S. Thorimbert, M. Malacria. *Angew. Chem. Int. Ed.*, **42**, 3404 (2003).
[21] Y.Q. Jiao, C. Qin, C.Y. Sun, K.Z. Shao, P.J. Liu, P. Huang, K. Zhou, Z.M. Su. *Inorg. Chem. Commun.*, **20**, 273 (2012).
[22] J.Q. Sha, J.W. Sun, C. Wang, G.M. Li, P.F. Yan, M.T. Li, M.Y. Liu. *CrystEngComm*, **14**, 5053 (2012).
[23] A.P. Karpinski, B. Makovetski, S.J. Russell, J.R. Serenyi, D.C. Williams. *J. Power Sources*, **80**, 53 (1999).

[24] H.S. Jia, W.S. Hou, L.Q. Wei, B.S. Xu, X.G. Liu. *Dent. Mater.*, **24**, 244 (2008).
[25] M. Bosetti, A. Massè, E. Tobin, M. Cannas. *Biomaterials*, **23**, 887 (2002).
[26] O. Choi, K.K. Deng, N.J. Kim, L. Ross, R.Y. Surampalli, Z.Q. Hu. *Water Res.*, **42**, 3066 (2008).
[27] Z.G. Han, Y.L. Zhao, J. Peng, H.Y. Ma, Q. Liu, E.B. Wang, N.H. Hu, H.Q. Jia. *Eur. J. Inorg. Chem.*, **2005**, 264 (2005).
[28] C. Streb, C. Ritchie, D.L. Long, P. Kögerler, L. Cronin. *Angew. Chem. Int. Ed.*, **46**, 7579 (2007).
[29] X.Y. Liu, H.L. Nie, L. Wang, R.D. Huang. *J. Coord. Chem.*, **66**, 444 (2013).
[30] J. Ruiz, M.E.G. Mosquera, G. García, E. Patrón, V. Riera, S. García-Granda, F. Van der Maelen. *Angew. Chem. Int. Ed.*, **42**, 4767 (2003).
[31] Q.G. Zhai, X.Y. Wu, S.M. Chen, Z.G. Zhao, C.Z. Lu. *Inorg. Chem.*, **46**, 5046 (2007).
[32] J.Q. Sha, J. Peng, H.S. Liu, J. Chen, A.X. Tian, P.P. Zhang. *Inorg. Chem.*, **46**, 11183 (2007).
[33] H.J. Pang, J. Peng, J.Q. Sha, A.X. Tian, P.P. Zhang, Y. Chen, M. Zhu. *J. Mol. Struct.*, **921**, 289 (2009).
[34] X.F. Kuang, X.Y. Wu, J.A. Zhang, C.Z. Lu. *Chem. Commun.*, **47**, 4150 (2011).
[35] Y.L. Xu, B.B. Zhou, Z.H. Su, K. Yu. *J. Coord. Chem.*, **64**, 3670 (2011).
[36] W.H. Chen, Z.B. Hu, Z.S. Zhang, Z.H. Qiu, Y.L. Zhou, J.H. Zhao, Q.L. Yuan, X.Y. Xiang, X.M. Wang. *Chin. J. Struct. Chem.*, **30**, 1178 (2011).
[37] W.H. Chen, Y. Xiang, Z.F. Chen, Q.M. Wu, Q.X. Zeng. *Acta Crystallogr., Sect. E: Struct. Rep. Online*, **63**, M2245 (2007).
[38] Z.B. Hu, Z.H. Qiu, W.H. Chen. *J. Cluster Sci.*, **24**, 1193 (2013).
[39] Z.B. Hu, W.H. Chen, J.X. Mi. *Chin. J. Struct. Chem.*, **32**, 1653 (2013).
[40] H.X. Yang, S.Y. Gao, J. Lü, B. Xu, J.X. Lin, R. Cao. *Inorg. Chem.*, **49**, 736 (2010).
[41] A.X. Tian, Z.G. Han, J. Peng, J.L. Zhai, B.X. Dong, J.Q. Sha. *J. Coord. Chem.*, **60**, 1645 (2007).
[42] H. Krishna, S.S. Krishnamurthy, M. Nethaji. *Inorg. Chim. Acta*, **362**, 38 (2009).
[43] H.B. Wu, Z.J. Huang, Q.M. Wang. *Chem. Eur. J.*, **16**, 12321 (2010).
[44] Z.G. Han, Y.N. Wang, J.J. Wu, X.L. Zhai. *Solid State Sci.*, **13**, 1560 (2011).
[45] H.J. Pang, J. Chen, J. Peng, J.Q. Sha, Z.Y. Shi, A.X. Tian, P.P. Zhang. *Solid State Sci.*, **11**, 824 (2009).
[46] Y.P. Chen, Y.Q. Wang, H.H. Zhang, Q.Y. Yang, R.Q. Sun, Y.N. Cao, L.Y. Zhao, C. Ni. *J. Mol. Struct.*, **883–884**, 103 (2008).
[47] G.M. Sheldrick. *Acta Crystallogr., Sect. A: Found. Crystallogr.*, **64**, 112 (2008).
[48] N.E. Brese, M. O'Keeffe. *Acta Crystallogr., Sect. B: Struct. Sci.*, **47**, 192 (1991).
[49] W. Sun, Y.X. Huang, Y.M. Pan, J.X. Mi. *J. Solid State Chem.*, **187**, 89 (2012).
[50] Y. Bai, G.Q. Zhang, D.B. Dang, P.T. Ma, H. Gao, J.Y. Niu. *CrystEngComm*, **13**, 4181 (2011).
[51] A.X. Tian, Z.G. Han, J. Peng, B.X. Dong, J.Q. Sha, B. Li. *J. Mol. Struct.*, **832**, 117 (2007).
[52] L.Z. Sun, W. Sun, W.J. Ren, J.Y. Zhang, Y.X. Huang, Z.M. Sun, Y.M. Pan, J.X. Mi. *J. Solid State Chem.*, **212**, 48 (2014).
[53] A.V. Knyazev, M. Mączka, N.N. Smirnova, L. Macalik, N.Y. Kuznetsova, I.A. Letyanina. *J. Solid State Chem.*, **182**, 3003 (2009).
[54] C.D. Wagner, W.M. Riggs, L.E. Davis, J.F. Moulder, G.E. Muilenberg. *Handbook of X-ray Photoelectron Spectroscopy*, Perkin Elmer Corp, Eden Prairie, MN (1978).
[55] I.A. Weinstock, J.J. Cowan, E.M.G. Barbuzzi, H.D. Zeng, C.L. Hill. *J. Am. Chem. Soc.*, **121**, 4608 (1999).
[56] S. Berchmans, R.G. Nirmal, G. Prabaharan, S. Madhu, V. Yegnaraman. *J. Colloid Interface Sci.*, **303**, 604 (2006).
[57] M. Sadakane, E. Steckhan. *Chem. Rev.*, **98**, 219 (1998).